RSC Advances

PAPER

View Article Online
View Journal | View Issue

Cite this: *RSC Adv.*, 2017, 7, 10559

A first-principles investigation of a new hard multi-layered MnB_2 structure†

Chunhong Xu, Kuo Bao, Shuailing Ma, Yanbin Ma, Shuli Wei, Ziji Shao, Xuehui Xiao, Xiaokang Feng and Tian Cui*

Received 22nd November 2016
Accepted 21st January 2017

DOI: 10.1039/c6ra27148k

rsc.li/rsc-advances

ReB_2-type MnB_2 has always been considered to be the ground-state structure of MnB_2. However, subsequent theoretical study has revealed that this structure is easy to decompose into elemental Mn and B under ambient conditions, which motivated us to look for a stable MnB_2 structure at high pressures. Using structure prediction algorithm USPEX and density functional theory calculations, we found a stable multi-layered MnB_2 structure with space group *Immm* at high pressure. The calculated hardness of *Immm*-MnB_2 is 22.5 GPa, which makes it a potential hard multifunctional material along with its conductive and magnetic properties. The hexagonal graphene-like boron networks of *Immm*-MnB_2 contribute to its hardness and stability.

1 Introduction

The research of transition-metal diborides (TMB_2s) never stops due to their outstanding physical and chemical properties, such as superconductivity, magnetism and superhardness, as well as being ultrahigh-temperature ceramics.[1–4] The design philosophy for hard transition-metal diborides makes them very resistant to shear deformation by introducing covalent bonds into highly incompressible metals.[5,6] Boron is a small and highly-bonded element,[7] which provides a covalent bond network in transition metal borides.[8] Recently, several transition-metal diborides, such as ReB_2,[9] OsB_2,[10] and TaB_2,[11] with a bulk modulus above 350 GPa, have been synthesized and greatly encouraged studies on transition metal diborides. Particularly, 3d magnetic metal manganese, with abundant valence electrons and "electron-deficient" boron, can form boron-based solids with the specific features of excellent multifunctional materials, such as high melting points, and magnetostructural and electronic behaviour.[12–14] Numerous studies, theoretical and experimental, have been conducted on MnB_2.[15–25] Originally, Binder and Post synthesized AlB_2–MnB_2 (SG *P*6/*mmm*) by heating mixtures of metal Mn and B at 1400–1500 °C.[19] Subsequently, in 2009, Aydin and Simsek predicted a superhard phase of MnB_2 with ReB_2-type structure (SG $P6_3/mmc$), which was regarded as the ground state of MnB_2 at ambient conditions.[16] In the same year, Jing Fan *et al.*[15] held the view that ReB_2-type MnB_2 could be synthesized only below 1020 K at ambient pressure. Unfortunately, after a prolonged endeavor, ReB_2-type MnB_2 was never successfully synthesized to date. More recently, Haiyang Niu, *et al.*[25] found ReB_2-type MnB_2 to be a metastable phase by variable-composition evolutionary algorithm calculations and first-principles calculations. Now that it is known that no stable MnB_2 phase exists at ambient pressure, it should be investigated whether there are novel phases of MnB_2 with new properties at high pressures. Thus, we investigated the structure, phase stability, electronic properties, and hardness of manganese diborides based on known transition-metal crystal structures and structure predictions. Through our calculations, a new high-pressure phase, *Immm*-MnB_2, was found. It is mechanically stable and can be quenched at ambient pressure. The electronic structure results indicate that *Immm*-MnB_2 is a metal and exhibits magnetic properties at ambient pressure, which could provide a new hard multifunctional material with a hardness of 22.5 GPa. Its hardness is mainly due to the strong covalent B–B bonds in the hexagonal graphene-like boron network.

2 Computational details

We performed evolutionary variable-cell simulations on Mn–B systems (at Mn : B ratios of 2 : 1, 1 : 1, 1 : 2, 1 : 3 and 1 : 4) with one to four formula units (FU) at moderate pressures of 0–60 GPa and zero temperature with the USPEX code.[26–28] We mostly applied spin-polarized first-principles calculations with the pseudo-potential plane-wave method using the Vienna *ab initio* simulation program (VASP) code.[29] The exchange and correlation effects were described by the generalized gradient approximation (GGA).[30] The valence electron configurations of manganese and boron are $3p^6 4s^2 3d^5$ and $2s^2 2p^1$, respectively. The bond lengths, cell parameters and atomic positions of any selected structure were fully optimized at different pressures

State Key Laboratory of Superhard Materials, College of Physics, Jilin University, Changchun, 130012, People's Republic of China. E-mail: cuitian@jlu.edu.cn

† Electronic supplementary information (ESI) available. See DOI: 10.1039/c6ra27148k

with a plane-wave cut-off energy of 500 eV and dense Monkhorst–Pack k-point meshes with a reciprocal space resolution of $2\pi \times 0.03$ Å^{-1}.[31] These settings enabled excellent convergence of the energy differences, stress tensors, and structural parameters. The elastic constants were calculated using the strain–stress method. The bulk modulus B, shear modulus G, B/G ratio and Poisson's ratio (ν) were estimated using the Voigt–Reuss–Hill (VRH) approximation.[32] In addition, we further derived phonon dispersions of the structures proposed by the USPEX with PHONOPY code.[33] The theoretical Vickers hardness was estimated using the Chen's model.[34]

3 Results and discussion

3.1 Thermodynamic stability and structural characteristics

In addition to the well-known hexagonal phase, ReB_2–MnB_2, we found a new high-pressure orthogonal phase, MnB_2, with space group *Immm* at about 50 GPa, which is clearly observed in the convex hull diagram. According to the latest Mn–B phase diagram,[18,24,25] the convex hull at different pressures including spin-polarization effects is shown in Fig. 1, connecting α-Mn,[35] α-B (0–19 GPa), and γ-B (19–89 GPa)[36] at $T = 0$ K. The formation enthalpy of Mn_xB_y is defined as follows: $\Delta H = H(Mn_xB_y) - xH(Mn) - yH(B)$. Our calculations indicate that the experimental AlB_2–MnB_2 and the pre-existing theoretical ReB_2–MnB_2 phase are metastable at ambient pressure (see Fig. 1a). Notably, when further increasing the pressure, the *Immm*-MnB_2 phase (proposed for the first time) can be synthesized at 50 GPa because its negative formation enthalpy lies in the convex hull[37,38] (Fig. 1b). Consequently, we can also obtain a phase transition of MnB_2 from ReB_2-type structure to *Immm* phase in the convex hulls.

As shown in Fig. 2a, we compared the enthalpies of typical transition-metal diborides (MoB_2-type MnB_2,[39] SG $R\bar{3}m$, WB_2-type MnB_2,[1] SG $P6_3/mmc$, OsB_2-type MnB_2,[40] SG *Pmmn*, RhB_2-type MnB_2,[41] SG $P2_1/m$), ReB_2–MnB_2 and *Immm*-MnB_2 as a function of pressure with respect to AlB_2-type MnB_2. As expected, the most thermodynamically stable structure is ReB_2-type MnB_2 at ambient pressure, which is in good agreement with previous first-principles calculations.[15,24] ReB_2-type MnB_2 is stable in the pressure range of 0–36.8 GPa. Above 36.8 GPa, the *Immm*-MnB_2 is the most energetically favorable up to 60 GPa. The results also show that *Immm*-MnB_2 can be obtained

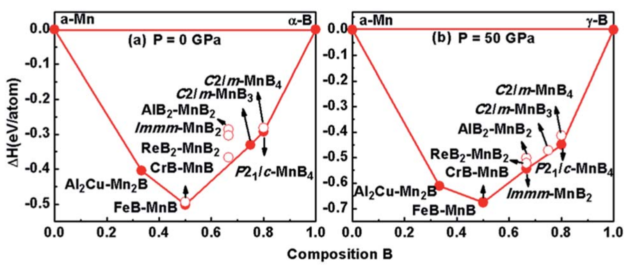

Fig. 1 Convex hull diagram of the Mn–B systems at pressures of 0 GPa (a) and 50 GPa (b). Solid circles represent stable phases, while hollow circles denote metastable phases.

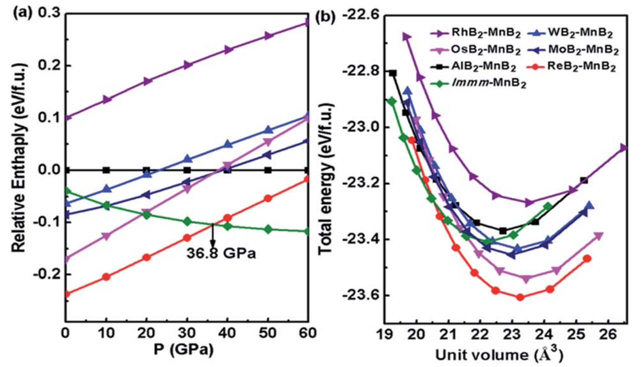

Fig. 2 (a) Computed relative enthalpy diagram of all the considered MnB_2 structures relative to AlB_2-type MnB_2 as a function of pressure. (b) Total energy per formula unit as a function of volume for the MnB_2 structures.

from Al_2Cu–Mn_2B + γ-B, FeB–MnB + γ-B, Al_2Cu–Mn_2B + $P2_1/c$-MnB_4 and FeB–MnB + $P2_1/c$-MnB_4 in the convex hulls. The energy–volume curves of the known MnB_2, illustrated in Fig. 2b, demonstrate a structural transition from ReB_2-type MnB_2 to *Immm*-MnB_2 within the pressure range considered.

The equilibrium lattice parameters of *Immm*-MnB_2 are a = 9.717 Å, b = 2.768 Å, c = 4.940 Å at ambient pressure. The orthogonal *Immm* structure contains six FUs per one unit cell with Mn atoms occupying the Wyckoff positions 2c (0.5, 0.5, 0) and 4e (0.6317, 0.5, 0.5) and B atoms occupying the 4j (0.5, 0, 0.6799) and 8m (0.6778, 0, 0.8205). From Fig. 3a and b, it can be clearly seen that *Immm*-MnB_2 is a multi-layered structure. However, unlike the common layered structure of graphene-like boron layers that sandwich metal layers along c-axis in transitional diborides, *e.g.* ReB_2, TaB_2, our predicted *Immm*-MnB_2 structure consists of hexagonal graphene-like boron networks formed by sp^2 hybridized B–B bonds and manganese layers in each layer along the b- and c-axis. Two of the B–B bonds in the hexagonal graphene-like boron networks of *Immm*-MnB_2, have a length of d_1 = 1.773 Å and four of them have a length of d_2 = 1.862 Å. The B–B bond between two adjacent six-membered boron rings has a distance of d_3 = 1.778 Å (see Fig. 3c). The shortest B–B bond length, of 1.773 Å, is shorter

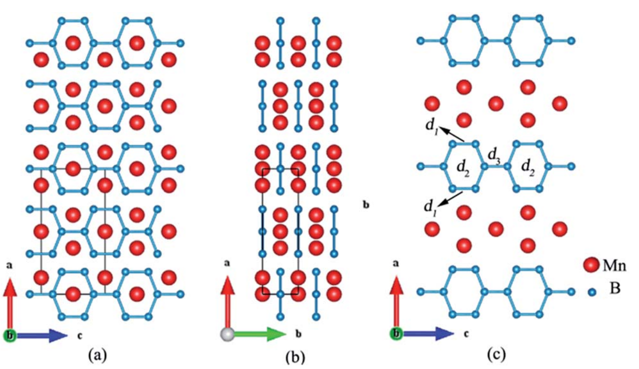

Fig. 3 Crystal structures of *Immm*-MnB_2: (a) along the b-axis, (b) along the c-axis. (c) View of a one-layer structure of *Immm*-MnB_2. The large red and small blue spheres represent Mn and B atoms, respectively.

than that of superhard ReB_2 (1.820 Å),[9] indicating a strong covalent bonding in *Immm*-MnB_2 at 0 GPa. In addition, the structural characteristics of *Immm*-MnB_2 are very similar to those of high-boron compounds, such as *Immm*-Mn_3B_4, suggesting that *Immm*-MnB_2 may have a strong stability and good mechanical properties.

3.2 Dynamical stability, mechanical stability and hardness

Evaluating the dynamical stability is necessary for assessing whether the proposed structure is stable or not. Thus, the phonon dispersion curves of *Immm*-MnB_2 at different pressures are displayed in Fig. 4. All the phonon modes of *Immm*-MnB_2 are positive in the entire Brillouin zone, which confirms its dynamic stability. *Immm*-MnB_2 was determined to be stable at 0–50 GPa, indicating that it can be obtained under ambient conditions.

Evaluating the mechanical properties of *Immm*-MnB_2 is necessary for determining its mechanical stability and industrial applications. The elastic constants (C_{ij}) for *Immm*-MnB_2 were calculated by the strain–stress method, and the results are presented in Table 1. For comparison with the predicted *Immm*-MnB_2 structure, we also calculated the elastic properties of some common transition-metal diborides such as TMB_2 (TM = Ta, W, Re), using the same approach, as summarized in Table S1 (ESI†). The corresponding elastic modulus (B, G, Y), B/G ratio, Poisson's ratio ν and hardness H_v of all the abovementioned diborides are summarized in Table 1.

From Table S1,† all the studied compounds are mechanically stable because the entire set of elastic constants C_{ij} satisfies the Born–Huang criterion.[45] Hence, the predicted *Immm*-MnB_2 could be mechanically stable at 0 and 50 GPa. By comparing the elastic constants of *Immm*-MnB_2, we can learn that the C_{11} (653 GPa) and C_{33} (643 GPa) are much larger than the C_{22} (442 GPa), implying that *Immm*-MnB_2 is relatively strong against compression along the *a*- and *c*-axis due to the hexagonal graphene-like boron networks. The computational results for TaB_2, WB_2 and ReB_2 are in good agreement with those of previous studies,[16,42–44] which proves the reliability of our calculations. As it is known, C_{44} is an important parameter that indirectly controls the hardness of materials. The *Immm*-MnB_2 phase has a C_{44} value of 273 GPa, which is comparable with that of ReB_2, indicating a relatively strong shear strength.[46] The calculated bulk modulus of *Immm*-MnB_2 is comparable to those of TaB_2,[42] WB_2 (ref. 43) and ReB_2,[44] suggesting that *Immm*-MnB_2 has a strong ability to prevent volume decrease (see Table 1). Moreover, *Immm*-MnB_2 has a shear modulus of 195 GPa, and

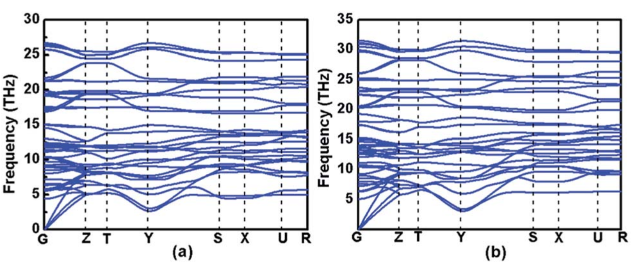

Fig. 4 Phonon dispersion curves of *Immm*-MnB_2 at (a) 0 GPa, and (b) 50 GPa along the high-symmetry directions of the Brillouin zone.

Table 1 Calculated bulk modulus B (GPa), shear modulus G (GPa), Young's modulus Y (GPa), B/G ratio, Poisson's ratio ν and hardness H_v (GPa) for *Immm*-MnB_2 and some common transition-metal diborides TMB_2 (TM = Ta, W, Re) at P = 0 and 50 GPa

Structure	P	B	G	Y	B/G	ν	H_v
Immm-MnB_2	0	308	195	483	1.58	0.24	22.5
	50	449	274	684	1.64	0.25	27.0
TaB_2	0	312	210	514	1.49	0.23	25.6
	0	308[a]	219[a]	531[a]	1.41[a]	0.21[a]	26.7[a]
WB_2	0	329	202	503	1.63	0.25	22.2
	0	320[b]	208[b]	512[b]		0.23[b]	
ReB_2	0	343	268	638	1.28	0.19	36.4
	0	344[c]	304[c]	642[c]	1.14[c]	0.21[c]	
	0	348[d]	295[d]	691[d]	1.18[d]	0.17[d]	35.9[d]

[a] Ref. 42. [b] Ref. 43. [c] Ref. 44. [d] Ref. 16.

hence it is reasonable to think that it could be a hard material, considering that its shear modulus is similar to that of conventional hard materials, such as TaB_2 and WB_2. In addition, the Poisson's ratio ν is indicative of the degree of directionality of the covalent bonding and greatly determines the hardness of materials. The Poisson's ratio of *Immm*-MnB_2 is 0.24, which is similar to that of TaB_2 and WB_2. This value lies between the covalently-bound materials' value of 0.1 and the value of 0.33 for materials with typically delocalized metal–metal bonds,[47] indicating a high degree of covalent and metallic bonding in the *Immm*-MnB_2 structure. The B/G ratio of a material represents its ductility or brittleness, with 1.75 being the critical value.[47] For *Immm*-MnB_2, the calculated B/G ratio is less than 1.75, implying that its brittle nature.

We calculated the hardness of *Immm*-MnB_2 using Chen's model: $H_v = 2(k^2G)^{0.585} - 3$.[34] The estimated hardness H_v of *Immm*-MnB_2 is 22.5 GPa at ambient pressure and 27.0 GPa at P = 50 GPa. Indeed, high pressure can enhance the mechanical properties of materials by increasing the elastic constants and elastic moduli. Compared to *Immm*-Mn_3B_4, with a hardness of 8.5 GPa,[25] our predicted structure is a relatively good hard material among common layered transition-metal diborides.

3.3 Electronic structure and magnetic properties

In order to explore the cause of the stability, hardness and magnetic properties of *Immm*-MnB_2, both the non-polarized and the spin-polarized electronic density of states (DOS) of *Immm*-MnB_2 at ambient pressure were calculated, and results are depicted in Fig. 5. As seen in Fig. 5, the calculated total density of states (TDOS) is dominated by Mn-d electrons due to their metallic character. This is the most evident feature of TM–B compounds at the Fermi level, and hence *Immm*-MnB_2 may be a good conductor. The energy range from −15 eV to −7.5 eV is primarily composed of B-s and B-p states, which indicates a strong interaction between B atoms. The overlapping at about −4.3 eV indicates covalency between the Mn-d and B-p states. The *Immm*-MnB_2 has a sharp peak at the Fermi level in non-polarized-DOS, which is a sign of magnetic instability (*i.e.*, the compounds will be more stable in a magnetic state).[48] According

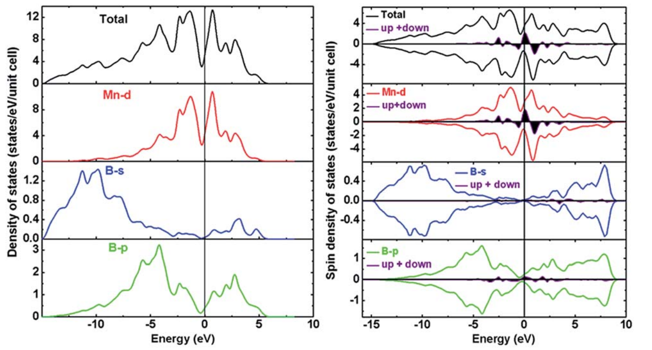

Fig. 5 Calculated total and partial DOS for *Immm*-MnB_2: (left panel) without spin-polarization, and (right panel) with spin-polarization. The vertical line at zero is the Fermi energy level. The area under the curves is the sum of spin-up and spin-down density of states.

to the Stoner model, spontaneous magnetization occurs when the condition $N_{TM}(E_F) \times I_{TM} > 1$ is satisfied, where $N_{TM}(E_F)$ is the non-polarized partial density of states of transition metal atoms at the Fermi level and I_{TM} is the exchange-correlation integral. The value of I_{TM} for Mn is 0.41 eV,[49] and hence the obtained result is 13.1 and larger than 1, indicating stable ferromagnetism. We also calculated the total energy *versus* volume for *Immm*-MnB_2, with and without spin-polarization, and we present the results in Fig. S1 (ESI†). The magnetic stability is confirmed once again by comparing the non-magnetic and magnetic total energy values calculated at the theoretical equilibrium volume.

The calculated spin-polarized total DOS of *Immm*-MnB_2 and partial DOS of Mn-d, B-s and B-p states are shown on the right panel in Fig. 5. According to our calculations, the results of the sum of the total spin-up and spin-down density of states (DOS) to the Fermi level reveal that *Immm*-MnB_2 is a magnetic material in which the local spin moment of Mn is 0.185 μ_B per atom, which is the same as the early experimental result on AlB_2–MnB_2 obtained by Andersson *et al.* (0.19 μ_B per atom).[50] The main ferromagnetic moment comes from the spin-polarized Mn-3d electrons. The magnetic moment in *Immm*-MnB_2 linearly decreases with increasing pressure, as shown in Fig. S2 (ESI†), indicating that the magnetic moment is affected by pressure modulation. In summary, the observation of strong B–B interactions in the hexagonal graphene-like boron network and the relatively strong Mn–B interactions are the main cause for the stability and hardness of *Immm*-MnB_2. Moreover, the presence of electrical conductivity and magnetic properties makes this multi-layered *Immm*-MnB_2 structure a potential multifunctional material.

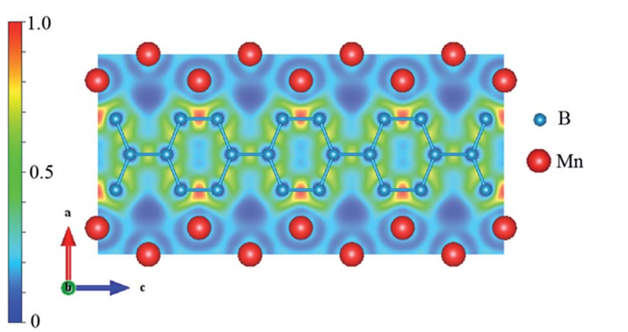

Fig. 6 Electron density map for *Immm*-MnB_2 in the (0 1 0) plane at 0 GPa.

3.4 Chemical bonding

In most studies on transition-metal borides, the strong covalent B–B bonds and the TM–B bonds are always the key factor for structural stability and hardness. Therefore, we calculated the electron localization function (ELF) and Bader charge to understand the nature of the B–B and Mn–B bonding. The spin-polarized ELF for *Immm*-MnB_2 at zero pressure is shown in Fig. 6. ELF = 1 corresponds to perfect electron-localization of covalent bonds, ELF = 0.5 corresponds to electron-gas-like pair probability, and ELF = 0 corresponds to perfect delocalization. As seen in Fig. 6, based on the ELF value, we can confirm the existence of strong covalent B–B bonding, particularly for the shortest B–B bond in the hexagonal graphene-like boron network, with a bond length of 1.773 Å, because of the high ELF value between this two boron atoms. C atoms have an electron configuration of $2s^22p^2$. Due to short bond lengths, the 2p orbitals can form π bonds, leading to the formation of graphene-like sheets.[51] Through Bader charge analysis (ESI†), it was found that there is much charge transfer from Mn to B. This promotes B^- ions to be isoelectronic to C, thus leading to the existence of hexagonal graphene-like boron networks. Meanwhile, the valence electrons of Mn are mostly transferred to B, which helps the 2p orbitals of B atoms to form π bonds. For *Immm*-MnB_2, the ELF is negligible at the Mn sites and attains maximum values between Mn and B atoms, very close to the B atoms, indicating partially covalent and metallic bonding features of the Mn–B bonds, *i.e.*, weak interactions between the Mn and B atoms. The B–B interactions are much stronger than the Mn–B interactions. From this, combined with the above-mentioned analysis of density of states, we can conclude that strong B–B bonds and relatively strong Mn–B bonds are the main cause of the hardness and stability of *Immm*-MnB_2.

4 Conclusion

In summary, we found a new multi-layered phase *Immm*-MnB_2, with a theoretical hardness of 22.5 GPa, by structure search based on the first-principles calculations. This phase is mechanically and dynamically stable at ambient pressure. By analyzing the elastic characteristics and electronic structure, we discovered that *Immm*-MnB_2 is a metal with magnetic properties, and has a magnetic moment of 0.185 μ_B/Mn, which makes it a promising hard multifunctional material.

The chemical bonding analysis of *Immm*-MnB_2 showed that the strong covalent B–B bonds in the hexagonal graphene-like boron network and the weak Mn–B interactions contribute to its hardness and stability. These results are important for understanding the structure and properties of magnetic transition-metal borides under high pressures and offer promise for the synthesis of magnetic transition-metal borides in the future.

Acknowledgements

This study was supported by the National Natural Science Foundation of China (No. 51632002, 51572108, 11634004, 11104103), the Program for Changjiang Scholars and the Innovative Research Team in University (No. IRT_15R23), the National Fund for Fostering Talents of Basic Science (No. J1103202),Some of the calculations were performed in the High Performance Computing Center (HPCC) of the Jilin University.

References

1 Q. Li, D. Zhou, W. T. Zheng, Y. M. Ma and C. F. Chen, *Phys. Rev. Lett.*, 2015, **115**, 185502.
2 J. Nagamatsu, N. Nakagawa, T. Muranaka, Y. Zenitani and J. Akimitsu, *Nature*, 2001, **410**, 63–64.
3 M. C. Cadeville, *J. Phys. Chem. Solids*, 1966, **27**, 667–670.
4 P. Rogl, *J. Less-Common Met.*, 1985, **110**, 283–294.
5 J. J. Gilman, R. W. Cumberland and R. B. Kaner, *Int. J. Refract. Hard Met.*, 2006, **24**, 1–5.
6 R. B. Kaner, J. J. Gilman and S. H. Tolbert, *Science*, 2005, **308**, 1268–1269.
7 B. Albert and H. Hillebrecht, *Angew. Chem., Int. Ed.*, 2009, **48**, 8640–8668.
8 T. P. Fehlner, *J. Solid State Chem.*, 2000, **154**, 110–113.
9 H. Y. Chung, M. B. Weinberger, J. B. Levine, A. Kavner, J. M. Yang, S. H. Tolbert and R. B. Kaner, *Science*, 2007, **316**, 436–439.
10 R. W. Cumberland, M. B. Weinberger, J. J. Gilman, S. M. Clark, S. H. Tolbert and R. B. Kaner, *J. Am. Chem. Soc.*, 2005, **127**, 7264–7265.
11 X. H. Zang, G. E. Hilmas and W. G. Fahrenholtz, *Mater. Lett.*, 2008, **62**, 4251–4253.
12 H. Y. Gou, A. A. Tsirlin, E. Bykova, A. M. Abakumov, G. V. Tendeloo, A. Richter, S. V. Ovsyannikov, A. V. Kurnosov, D. M. Trots, Z. Konôpková, H.-P. Liermann, L. Dubrovinsky and N. Dubrovinskaia, *Phys. Rev. B: Condens. Matter Mater. Phys.*, 2014, **89**, 064108.
13 Y. C. Liang, X. Yuan, Y. F. Gao, W. Q. Zhang and P. H. Zhang, *Phys. Rev. Lett.*, 2014, **113**, 176401.
14 R. O. Zaitsev and N. V. Terekhina, *J. Exp. Theor. Phys.*, 2002, **94**, 367–376.
15 J. Fan, K. Bao, X. L. Jin, X. X. Meng, D. F. Duan, B. B. Liu and T. Cui, *J. Mater. Chem.*, 2012, **22**, 17630–17635.
16 S. Aydin and M. Simsek, *Phys. Rev. B: Condens. Matter Mater. Phys.*, 2009, **80**, 134107.
17 S. Khmelevskyi and P. Mohn, *Solid State Commun.*, 2000, **113**, 509–512.
18 H. Okamoto, *J. Phase Equilib.*, 1993, **14**, 121–122.
19 I. Binder and B. Post, *Acta Crystallogr.*, 1960, **13**, 356.
20 X. X. Meng, K. Bao, P. W. Zhu, Z. He, Q. Tao, J. J. Li, Z. P. Mao and T. Cui, *J. Appl. Phys.*, 2012, **111**, 112616.
21 G. Y. Gou, G. S. Neumann, E. Bykova, Y. Nakajima, N. Miyajima, Y. Li, S. V. Ovsyannikov, L. S. Dubrovinsky and N. Dubrovinskaia, *Appl. Phys. Lett.*, 2013, **102**, 061906.
22 R. Kiessling, *Acta Chem. Scand.*, 1950, **41**, 46–159.
23 P. Vajeeston, P. Ravindran, C. Ravi and R. Asokamani, *Phys. Rev. B: Condens. Matter Mater. Phys.*, 2001, **63**, 045115.
24 B. Wang, X. Li, Y. X. Wang and Y. F. Tu, *J. Phys. Chem. C*, 2011, **115**, 21429–21435.
25 H. Y. Niu, X. Q. Chen, W. J. Ren, Q. Zhu, A. R. Oganov, D. Z. Li and Y. Y. Li, *Phys. Chem. Chem. Phys.*, 2014, **16**, 15866–15873.
26 A. O. Lyakhov, A. R. Oganov, H. T. Stokes and Q. Zhu, *Comput. Phys. Commun.*, 2013, **184**, 1172–1182.
27 A. R. Oganov, A. O. Lyakhov and M. Valle, *Acc. Chem. Res.*, 2011, **44**, 227–237.
28 A. R. Oganov and C. W. Glass, *J. Chem. Phys.*, 2006, **124**, 244704.
29 G. Kresse and J. Furthmüller, *Phys. Rev. B: Condens. Matter Mater. Phys.*, 1996, **54**, 11169–11186.
30 J. P. Perdew, K. Burke and M. Ernzerhof, *Phys. Rev. Lett.*, 1996, **77**, 3865–3868.
31 H. J. Monkhorst and J. D. Pack, *Phys. Rev. B: Solid State*, 1976, **13**, 5188–5192.
32 R. Hill, *Proc. Phys. Soc., London, Sect. A*, 1952, **65**, 349–354.
33 A. Togo, F. Oba and I. Tanaka, *Phys. Rev. B: Condens. Matter Mater. Phys.*, 2008, **78**, 134106.
34 X. Q. Chen, H. Y. Niu, D. Z. Li and Y. Y. Li, *Intermetallics*, 2011, **19**, 1275–1281.
35 A. C. Lawson, A. C. Larson, M. C. Aronson, S. Johnson, Z. Fisk, P. C. Canfield, J. D. Thompson and R. B. Von Dreele, *J. Appl. Phys.*, 1994, **76**, 7049–7051.
36 A. R. Oganov, J. H. Chen, C. Gatti, Y. Z. Ma, Y. M. Ma, C. W. Glass, Z. X. Liu, T. Yu, O. O. Kurakevych and V. L. Solozhenko, *Nature*, 2009, **457**, 863–867.
37 G. Ghosh, A. van de Walle and M. Asta, *Acta Mater.*, 2008, **56**, 3202–3221.
38 X. W. Zhang, G. Trimarchi and A. Zunger, *Phys. Rev. B: Condens. Matter Mater. Phys.*, 2009, **79**, 092102.
39 S. Okada, T. Atoda, I. Higashi and Y. Takahashi, *J. Mater. Sci.*, 1987, **22**, 2993–2999.
40 B. Aronsson, E. Stenberg and J. Åselius, *Nature*, 1962, **195**, 377–378.
41 B. H. Chu, D. Li, F. B. Tian, D. F. Duan, X. J. Sha, Y. Z. Lv, H. D. Zhang, B. B. Liu and T. Cui, *Sci. Rep.*, 2015, **5**, 10500.
42 W. J. Zhao and Y. X. Wang, *J. Solid State Chem.*, 2009, **182**, 2880–2886.
43 X. F. Hao, Y. H. Xu, Z. J. Wu, D. F. Zhou, X. J. Liu, X. Q. Cao and J. Meng, *Phys. Rev. B: Condens. Matter Mater. Phys.*, 2006, **74**, 224112.
44 Y. X. Wang, *Appl. Phys. Lett.*, 2007, **91**, 101904.
45 Z. J. Wu, E. J. Zhao, H. P. Xiang, X. F. Hao, X. J. Liu and J. Meng, *Phys. Rev. B: Condens. Matter Mater. Phys.*, 2007, **76**, 054115.
46 M. M. Zhong, X. Y. Kuang, Z. H. Wang, P. Shao, L. P. Ding and X. F. Huang, *J. Phys. Chem. C*, 2013, **117**, 10643–10652.
47 S. F. Pugh, *Philos. Mag.*, 1954, **45**, 823–843.
48 S. Kervan, *J. Supercond. Novel Magn.*, 2011, **24**, 815–818.
49 J. F. Janak, *Phys. Rev. B: Solid State*, 1977, **16**, 255.
50 L. Andersson, B. Dellby and H. P. Myers, *Solid State Commun.*, 1966, **4**, 77–78.
51 M. J. Rice, A. R. Bishop and D. K. Campbell, *Phys. Rev. Lett.*, 1983, **51**, 2136.